

Supplementary Materials for

An Insight into the Battery Degradation for a Proposal of a Battery Friendly Charging Technique

Bikash Sah,¹ Praveen Kumar,^{1*}

¹Department of Electronics and Electrical Engineering, Indian Institute of Technology Guwahati,
Guwahati, Assam, 781039, India

*Correspondence to: E-mail: praveen_kumar@iitg.ac.in

This PDF file includes:

1. Supplementary Text
2. Supplementary Figures
3. Supplementary Tables

1 Supplementary Text

1.1 Doyle Fuller Newman Model of Li-ion battery

This subsection provides the equations and their boundary conditions used in this work. The Doyle Fuller Newman Model (DFN), based on volume averaging and a standard model for Li-ion batteries, is used¹⁻³. Fig. 1 shows the model of the battery with all the components, viz., negative electrode, separator, and positive electrode. The subscripts n,s, and p are used to denote variables related to negative electrode, separator, and positive electrode, respectively and $k \in \{n, s, p\}$. Further, 'e' and 's' are added as a subscript to denote the electrolyte variables and solid-phase variables, respectively.

Table S1 Symbols used in the model: The symbols used in mathematical equations for modelling are presented. The -ve=Negative, and +ve=Positive are used in the table for ease.

Parameter	Symbol
thicknesses of the -ve electrode	L_n
thicknesses of the separator	L_s
thicknesses of the +ve electrode	L_p
distance between the -ve and +ve current collectors	$L = L_n + L_s + L_p$
radius of -ve active material particles	R_n
radius of +ve active material particles	R_p
location through the thickness of the battery	$x \in [0, L]$
location within each particle of active material	$r \in [0, R_k], \quad k \in \{n, p\}$
-ve electrode regions (Ω_n)	$[0, L_n]$
separator regions (Ω_s)	$[L_n, L - L_p]$
+ve electrode regions (Ω_p)	$[L - L_p, L]$
electric potentials	ϕ
current densities	i
lithium-ion concentrations in electrolyte	c
molar fluxes	N
macroscopic spatial variable	x
microscopic spatial variable	r
time	t
Q : heat source, W	c_p
molecular weight, kgmol^{-1}	M
heat source, W	Q

Considering the definition of all the subscript and the symbols, the governing equations of the DFN are given below. The governing equations are categorised as charge conservation, molar conservation, and the respective electrochemical reactions.

1.1.1 Governing equations

Charge conservation:

$$i_{e,k}^x = \begin{cases} a_k j_k, & k = n, p, \\ 0, & k = s, \end{cases} \quad k \in \{n, s, p\},$$

$$i_{e,k} = \varepsilon_k^b \kappa_e(c_{e,k}) \left(-\phi_{e,k}^x + 2(1-t^+) \frac{RT}{F} x (\log(c_{e,k})) \right), \quad k \in \{n, s, p\},$$

$$I - i_{e,k} = -\sigma_k \phi_{s,k}^x, \quad k \in \{n, p\}.$$

Molar conservation:

$$\varepsilon_k c_{e,k} t = N_{e,k}^x + \frac{1}{F} i_{e,k}^x, \quad k \in \{n, s, p\},$$

$$N_{e,k} = \varepsilon_k^b D_e(c_{e,k}) c_{e,k}^x + \frac{t^+}{F} i_{e,k}, \quad k \in \{n, s, p\},$$

$$c_{s,k} t = \frac{1}{(r)^2} r \left((r)^2 D_{s,k} c_{s,k} r \right), \quad k \in \{n, p\}.$$

Electrochemical reactions:

$$j_k = j_{0,k} \sinh \left(\frac{F \eta_k}{2RT} \right), \quad k \in \{n, p\},$$

$$j_{0,k} = m_k (c_{s,k})^{1/2} (c_{s,k,\max} - c_{s,k})^{1/2} (c_{e,k})^{1/2} \quad k \in \{n, p\},$$

$$\eta_k = \phi_{s,k} - \phi_{e,k} - U_k(c_{s,k}|_{r=R_k}), \quad k \in \{n, p\}.$$

Lumped thermal model of cell:

The energy conservation of the cell is defined using:

$$m c_p \frac{dT}{dt} = \dot{Q} + hA (T_\infty - T)$$

Definition of boundary conditions:

Current:

$$i_{e,n}|_{x=0} = i_{e,p}|_{x=L} = 0,$$

$$\phi_{e,n}|_{x=L_n} = \phi_{e,s}|_{x=L_n}, \quad i_{e,n}|_{x=L_n} = i_{e,s}|_{x=L_n} = I,$$

$$\phi_{e,s}|_{x=L-L_p} = \phi_{e,p}|_{x=L-L_p}, \quad i_{e,s}|_{x=L-L_p} = i_{e,p}|_{x=L-L_p} = I.$$

Concentration in electrolyte:

$$N_{e,n}|_{x=0} = 0, \quad N_{e,p}|_{x=L} = 0,$$

$$c_{e,n}|_{x=L_n} = c_{e,s}|_{x=L_n}, \quad N_{e,n}|_{x=L_n} = N_{e,s}|_{x=L_n},$$

$$c_{e,s}|_{x=L-L_p} = c_{e,p}|_{x=L-L_p}, \quad N_{e,s}|_{x=L-L_p} = N_{e,p}|_{x=L-L_p}.$$

Concentration in the electrode active material:

$$c_{s,k} r \Big|_{r=0} = 0, \quad -D_{s,k} c_{s,k} r \Big|_{r=R_k} = \frac{j_k}{F}, \quad k \in \{n, p\}.$$

Reference potential

$$\phi_{s,n}|_{x=0} = 0.$$

Initial conditions

$$c_{s,k}(x, r, 0) = c_{s,k,0},$$

$$c_{e,k}(x, 0) = c_{e,typ},$$

The models related to the degradation phenomenon (SEI layer growth, Li-plating, particle cracking, inactive material formation, and other derivatives) are presented in the main manuscript in section 1.3.

1.2 Inactive material concentration

Li-ion batteries have active and inactive materials. Those materials that contribute to the energy storage process, such as storing lithium, are the active materials. The inactive materials include separator, binders, current collectors, electrolytes, additives and packaging components^{4,5}. These inactive materials constitute almost 60% of the battery weight and hence, are a crucial parameter affecting the battery energy and power density⁶. The concentration of inactive materials keeps increasing with the age of the battery. The side reactions in the battery are a major cause supporting the conversion of active materials to inactive^{4,7,8}.

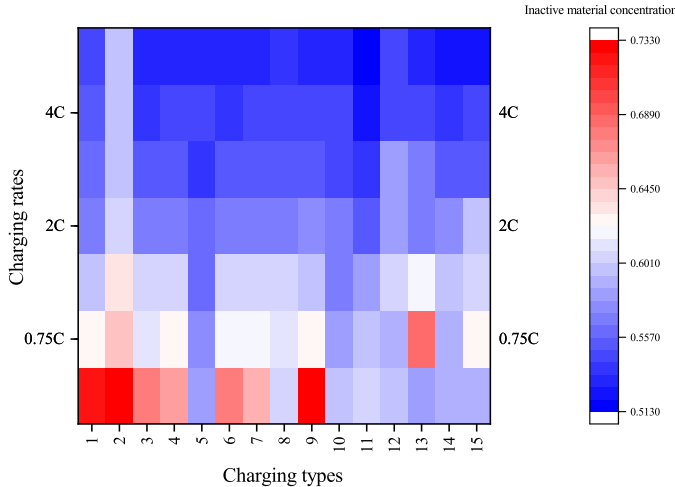


Fig. S1 The variation of X-averaged negative electrode inactive material volume fraction when the elected battery is charged using different types of charging techniques at different C_{rate} is shown. The lower charging rates result in the maximum formation of inactive materials because chemical degradation dominates at lower C_{rate} .

Fig. S1 shows the formation of inactive material in the battery when different types of charging are used at different charging rates. The inactive material formation is the highest at lower charging rates. The charging technique 1 (CC), 2 (CCCV) and 9 (pulse charge with discharge) shows the highest concentration of inactive material at the end of 350 cycles of charge and discharge at low discharging rates. With an increase in the charging rates,

the amount of inactive material concentration is reduced. The reduction in the formation of inactive material is related to two primary reasons: i) the battery reaches the cutoff potential faster because of the increased overpotential, and ii) the time to charge is reduced. The first reason is, a higher C_{rate} leads to an increase in chemical kinetics, charge transfer via diffusion and change in equilibrium potential. Since the overpotential is high, the cutoff voltage is reached faster, and the battery is considered to be charged. A larger time frame to charge at a slower C_{rate} leads to a larger time for side reactions. Hence, the concentration of inactive materials is higher at slow C_{rate} .

CCCV and variants of pulse charging have shown reasonable changes in the concentration of inactive material formation. During CCCV, although the battery is charged at high currents during initial states, the charging end with a reduction in the C_{rate} or fall of charging current to 50 mA during CV mode. Hence, CCCV is the only technique in which there is the least variation in the concentration of inactive material followed by pulse charging with discharge (charging types 12 and 13). Fig. S1 shows the impact of the duty cycle, rest time and the amplitude of discharge pulse in different variants of pulse charging. The rest period during the pulse charge provides a settling time for the batteries. During the settling time, the increase in the chemical kinetics, charge transfer rate, and change in equilibrium potential is reduced or halted. Hence, the formation of inactive material is also less when compared to CC and CCCV. However, there are variations due to the parameters of the pulses. The interpretation of the concentration of inactive material for pulse charging without discharge is shown in charging types 3 to 8. The decrease in the concentration of inactive material is seen with a reduction of the t_{on} . For a higher t_{on} , the charging technique tends to behave like CC or CCCV; hence, a similar concentration is seen, although it is less than CC and CCCV. The t_{off} also impacts the formation of inactive materials. A reduction in the t_{off} leads to a reduction in the formation of inactive material. In general, a reduced t_{on} and t_{off} reduces the increase in the concentration of inactive material volume concentration.

The pulse charging with discharge leads to the least increase in the concentration of inactive material compared to CC, CCCV and pulse charge without discharge. Charge type 9 to 15 in Fig. S1 shows the variation of the concentration of inactive material. The charge types 9, 10 and 11 have a reduction of t_{on} for a constant t_{off} and discharge time, resulting in reduced inactive material concentration. The results obtained follow a similar trend as observed in pulse charging without discharge. Further investigation on the impact of discharge pulse is studied by changing the amplitude. For simulations in which the amplitude of discharge current is equal to the average current, but the on-time varies from highest to lowest (charge type 9, 10 and 11), the inactive material concentration is least for the smallest t_{on} . When the amplitude of the discharge

current is reduced to half of the average current, higher on-time results in the formation of less inactive material. In contrast, when the amplitude of the discharge pulse is double the average current, inactive material volume concentration is more for a higher on-time. Hence, for pulse charging with discharge, with charge type in which the amplitude of discharge current equals the average current and has the least on-time results in the formation of the least inactive material. The battery discharge process also renders a similar change in the equilibrium potential of the reactions in the batteries. Hence, an increase in the discharge pulse leads to a rise in the formation of inactive materials.

1.3 Reaction overpotential

The deviation of the battery potential from the electrode equilibrium potential to meet the requirements of current during charge or discharge is commonly called overpotential. A simplistic example of overpotential can be visualised by observing the increase in the terminal voltage of a battery when a charger is connected to it after allowing it to rest for an hour or more. Hence, a higher charge or discharge current will lead to an increase in the overpotential of the battery. Different types of overpotential are described in the literature. Those include thermodynamic, charge-transfer, ohmic and concentration overpotential. Splitting the overall overpotential is not done in this work. The literature describes that an increase in the SEI layer thickness (ohmic overpotential) adds to the increase in the overpotential⁹.

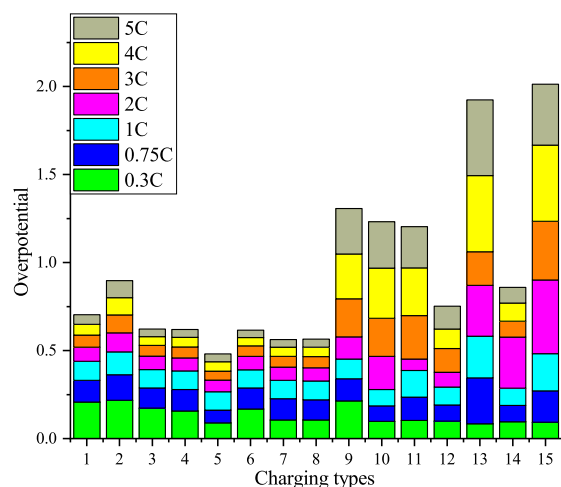


Fig. S2 The variation of X-averaged negative electrode reaction overpotential [V] when the battery is charged using different charging techniques at different C_{rate} is shown.

Fig.S2 shows the changes in the overpotential with an increase in the charging rates and change in the charging types. During CC and CCCV, the highest overpotential is seen during low C_{rate} . Since at low C_{rate} , the SEI formed is stable and thick, the ohmic overpo-

tential due to SEI layer formation is dominant. Further, CCCV have higher overpotential when compared to CC, which is similar to the SEI layer thickness. Moving right in Fig.S2, the variation of overpotential when variants of pulse charging are done is described. The rise in the overpotential is the least in CT5, which is attributed to SEI layer formation. With the decrease in t_{on} and t_{off} , the rise in overpotential decreases. The rest period in the pulse charge provided time to settle. Hence, the overpotential due to thermodynamics, charge transfer, and concentration reduces. Further, the growth of the SEI layer is also constrained due to the least deviation from equilibrium potential.

The pulse charging without discharge is found to reduce the rise in the overpotential. However, when the pulse charging with discharge is observed, a sudden increase in the overpotential is visible. Although the rise in the overpotential follows the trend of decreasing t_{on} , the SEI layer thickness is not the highest compared to Fig. 3 (a). Hence, in pulse charge with discharge, it is not the ohmic overpotential that dominates; it is the thermodynamics and the charge transfer overpotential that dominates. The claim is corroborated by the rise in cell temperature as seen in Fig. 3 (c). The charge transfer overpotential increases with an increase in the C_{rate} . Hence, with an increase in the amplitude of the discharge pulse, from half of the average charging current to double the charge current, the overpotential rises. Both thermodynamic and charge transfer overpotential dominates the rise in overpotential when pulse charging with discharge is performed with a higher amplitude discharge pulse. CT5 and CT8 resulted in the best charging types when the increase in overpotential is accounted for.

1.4 Extent of lithiation

Lithiation is the intercalation of Li-ions in the negative electrode during charging. The extent of lithiation happening prominently impacts the capacity of the battery during charging. The formation cycle, which is done after the manufacturing of the battery, involves the process of prelithiate anode, which is also accompanied by SEI layer formation and a rise in overpotential during formation. Hence, the extent of lithiation is also related to SEI layer thickness and overpotential¹⁰. Fig. S3 shows the variation of lithiation at different charging techniques and rates.

The change in the extent of lithiation in CCCV is the least for different charging rates. A larger impact of C_{rate} is seen in CC. The process of lithiation is dependent on the ease of intercalating the electrodes. The ease of intercalating further depends on the diameter of the pores. With the growth of the SEI layer, the diameter decreases and adds resistance to the diffusion of ions. Hence, lithiation reduces with the ageing of the battery. At the lower C_{rate} , the SEI layer formed is thick and stable; hence, lithiation reduces.

On the contrary, although the SEI layer is less thick than the

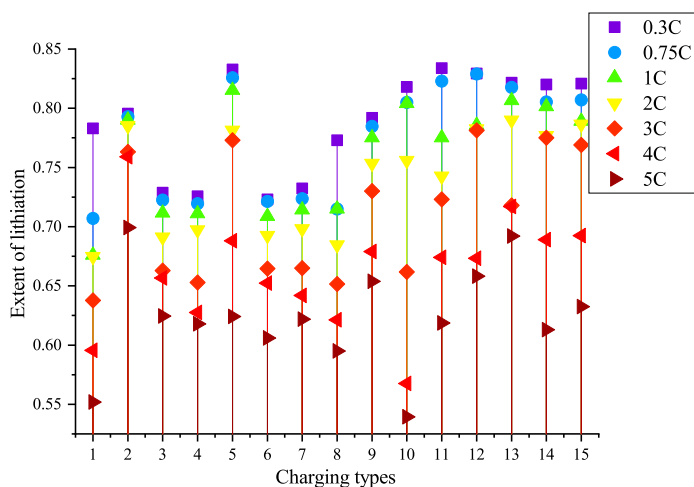


Fig. S3 The X-averaged negative electrode extent of lithiation for different types of charging and at different C_{rate} is shown. Lower C_{rate} results in better lithiation while higher C_{rate} reduces it. A better lithiation is related to overpotential and chemical kinetics, which impact the settlement of ions in electrodes.

lower C_{rate} , the lithiation is less in the higher C_{rate} . Hence, there are other factors also that impact the extent of lithiation. The higher C_{rate} leads to an increase in the chemical kinetics in the battery. The equilibrium potential and overpotential also increase with an increase in the cell temperature. The overall change in the battery makes does not allow the Li-ion to settle in and stimulate various side reactions.

A few patterns of pulse charging show better results when compared to conventional CC and CCCV. The variation of t_{on} and t_{off} shows similar changes in the variation of the extent of lithiation. A decrease in the t_{on} and t_{off} leads to better lithiation. A larger t_{on} allows accumulative growth of the SEI layer and cell temperature, and the t_{off} helps to settle the processes in the battery. A reduction in t_{on} time ensures a reduction in the accumulative growth of the SEI layer and temperature. The pulse charging with discharge good results in low charging rates, but the extent of lithiation reduced drastically at higher charging rates. The decrease in t_{on} is visible here as well, with improvement in the extent of lithiation. The amplitude of the discharge pulse also impacts the lithiation, but visible changes are seen only at higher C_{rate} . At higher C_{rate} , the impact of SEI layer thickness and the processes leading to an increase in temperature dominates convolutes. However, the impact of the SEI layer is dominant only at low C_{rate} .

1.5 Porosity

The porosity of the electrodes is an important parameter that impacts the capacity of the Li-ion battery. The porosity of pores in the electrode is varied with the deposition of inactive materials, which is the SEI layer. With an increase in the thickness of the

SEI layer, the accessible active surface area gets reduced, leading to a reduction in the intercalation reactions, as discussed in previous subsections.^{11,12}. Hence, the porosity also varies similarly to the inactive material, and SEI layer thickness varies. Fig. S7b shows the variation of porosity of the negative electrode after 350 charge-discharge cycles. The porosity is the least in the case of CCCV and CC, followed by CT9. The variation in porosity in Fig. S7b demonstrates that changes in charging types have an impact on the performance of the battery, especially when looking into the variants of pulse charging.

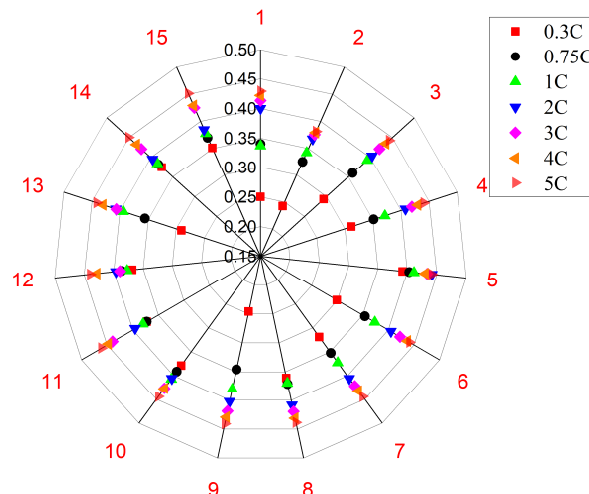


Fig. S4 The X-averaged negative electrode porosity for different types of charging and at different C_{rate} is shown. The porosity depends on the SEI layer thickness over particles in electrodes. Hence, at lower C_{rate} , when SEI layer thickness increases, the porosity of the electrodes is also reduced.

The porosity impacts from the t_{on} and t_{off} for pulse charge without discharge. It is observed that for a lower value of on-time, the impact on the porosity is the least and retains a higher value. A lower off-time, too, has a similar impact on the porosity. Charge type 5 shows the least variation in the porosity for different charge rates. With an increase in the C_{rate} , the change in the value of porosity is reduced. In contrast, a lower charging rate leads to a higher reduction of porosity with an increase in the number of cycles. As described in previous subsections, the SEI layer formed is thicker and stable at lower charging rates. Hence, porosity is reduced drastically, and the impact of pulse charging is also negligible. The pulse charging without discharge is capable of controlling the reduction in the porosity of the negative electrode. However, pulse charge with the discharge has shown similar benefits when the variation of t_{on} and t_{off} is investigated.

The variation of pulse charging with discharge is shown in charge types 9 to 15. The change in the porosity is reduced with the use of pulse charge with discharge because of the reduction in

the SEI layer thickness, as shown in Fig. 3 (a). The decrease in the t_{on} in this technique also impacts the porosity. For a higher value of on-time, the change in the porosity is greater at lower charging rates. For higher charging rates, the change in porosity is the least. The charge types- 9, 10, and 11 show a reduction in the change in the porosity because of the reduction in t_{on} . The reduction in t_{on} stops a consistent rise in the rate of side reactions, and the t_{off} allows to settle processes. The amplitude of the discharge pulse also impacts the change in the porosity of the electrodes. For cases where the amplitude of the discharge pulse is equal to the average current, the difference in porosity is with the reduction in t_{on} , the change in the porosity reduces. On the contrary, a more significant change in porosity is found when the amplitude of the discharge current is equal to half of the average current.

A larger difference in porosity is observed in case the amplitude of the discharge current is double the average current. The change in the porosity is related to the equilibrium potential, which on the increase in magnitude, falls below the stability limits of the electrolyte leading to SEI formation. The rest period after the discharge pulse helps to stabilise the SEI layer. Hence, in the case of low C_{rate} , which also generates a stable SEI layer, the larger reduction in porosity is visible even when pulse charging with discharge is used.

1.6 Tortuosity

Tortuosity is an important factor relating to the mass and charge transport in an electrochemical device¹³. Although this factor plays a major role in the fast charging of batteries, it has not been widely discussed in works dealing with the capacity fade of batteries. Tortuosity is a microstructural characteristic that defines the ease of flow of ions during charging and discharging¹⁴⁻¹⁶. However, tortuosity should not be misunderstood with the geometric property of microstructure but rather interpreted as the effective diffusibility of mass in a porous object¹³. A higher value of tortuosity infers that the travel path through the porous structure is not smooth or short for the charge. Hence, the lower the value of tortuosity, the better the charge and mass transport in the battery's electrodes¹⁶.

Fig. S5 shows the variation of values of tortuosity for different types of charging at various C_{rates} . The lower charging rates in all the techniques showed resulted in the highest value of tortuosity. The conventional CC and CCCV have the maximum variation in the tortuosity, especially at low C_{rate} . At lower C_{rate} other parameters such as the concentration of inactive materials and the SEI layer thickness are higher. The SEI layer is a type of inactive material that is formed on the surface of electrode particles. These particles are kept together using binders and have spaces in between them, which are called pores. These pores allow the Li-ion to settle during intercalation reaction or charging. When the SEI layer

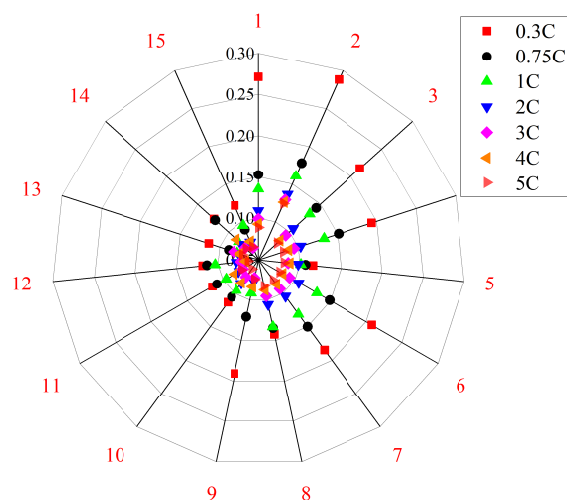


Fig. S5 The X-averaged negative electrode tortuosity for different types of charging and C_{rate} is shown. Tortuosity is inversely related to porosity. Hence, the variation follows a trend but is opposite to the porosity.

thickness increases, the pores start getting clogged and restrain the movement of charges^{11,13}. Hence, during charge transfer or diffusion, a larger path is required, which leads to an increase in tortuosity. Since the porosity of electrodes is related to tortuosity, the calculation also involves the value of porosity.

On the introduction of pulse charge techniques, the change in the values of tortuosity reduces as compared to CC and CCCV. The t_{on} and t_{off} have an impact on the change in the tortuosity similar porosity changes shown in Fig. S7b. The decrease in the t_{on} and t_{off} reduces the tortuosity changes due to similar reasons as described in the previous subsection explaining the less change in the porosity and SEI layer thickness. Looking at the pulse charging with discharge, the change in tortuosity over different charging rates is the least except for a low C_{rate} in CT9. CT9 has a high t_{on} , therefore at low C_{rate} , the formation of SEI to constrain the diffusivity of charge is least. On an increase of C_{rate} , the internal cell temperature increases, boosting the diffusivity of charge. Further, the increase in the amplitude of the discharge pulse in pulse charging with discharge also increases the internal cell temperature. Hence, for CT13 and CT15, in which the amplitude of the discharge pulse is twice the average charge current, the tortuosity changes are minimal. The pulse charge with discharge turns out to be a good alternative to fast charge batteries if only tortuosity is considered under study.

2 Supplementary Figures

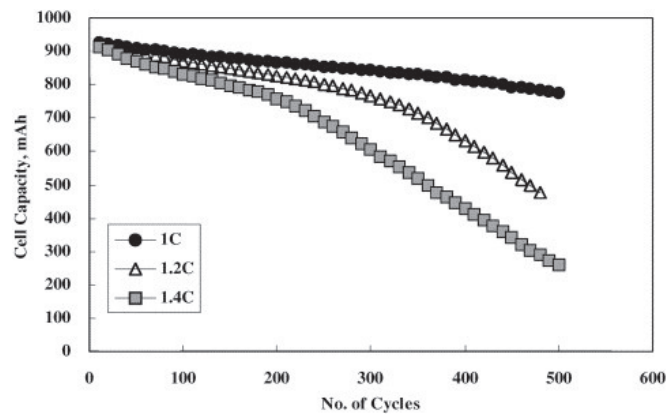


Fig. S6 The acceleration of capacity fade with an increase in charging rate as described in⁹

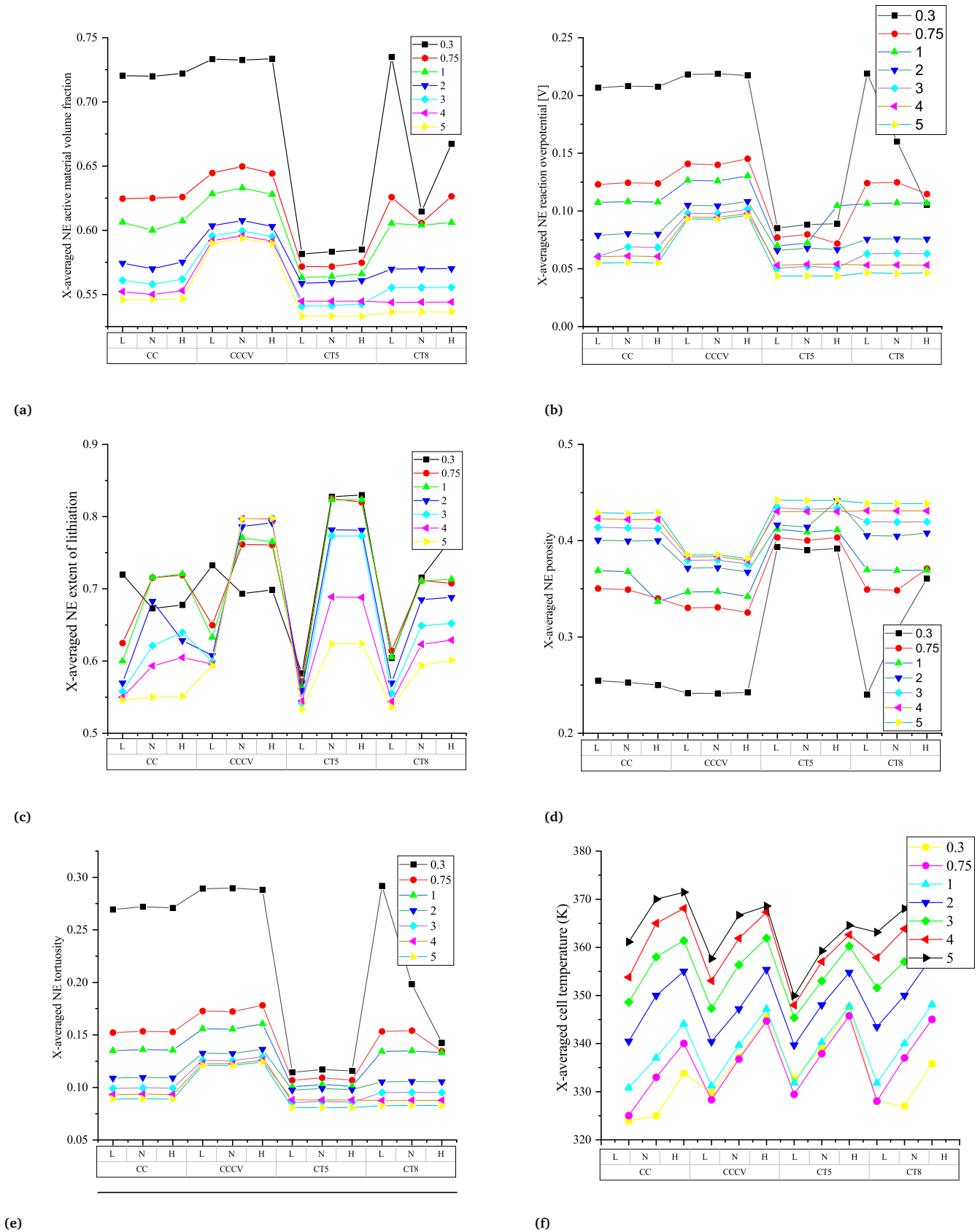


Fig. S7 Variation of different parameters of the batteries: (a) X-averaged negative electrode inactive material volume fraction; (b) X-averaged negative electrode reaction overpotential [V]; (c) X-averaged negative electrode extent of lithiation; (d) X-averaged negative electrode porosity; (e) X-averaged negative electrode tortuosity; (f) X-averaged cell temperature (K). For each parameter, shown in the figure, CT5 results in a value which helps to constrain the battery degradation.

3 Supplementary Table

Table S2 The table shows the parameters of cells used for simulating the different types of charging at different rates. The cell parameters are taken from^{8,17–21} and the additional data required for the degradation models are those predefined in PyBaMM.

Parameter	Units	Anode	Cathode
Length of the electrode	μm	88	80
Conductivity of electrode	S/m	100	100
Volume fraction of solid phase		0.49	0.59
Volume fraction of liquid phase		0.485	0.385
Film thickness	μm	2	2
Maximum Li ion in sold phase	mol/m^3	30555	51555
State of charge		0.03	0.95
Diffusion coefficient of solid phase	m^2/s	3.9×10^{-14}	1×10^{-14}
Rate constant of electrochemical reactions	$\text{A}/\text{m}^2/(\text{mol}/\text{m}^3)^{3/2}$	4.854×10^{-6}	2.252×10^{-6}
Anodic transfer coefficient of electrochemical reactions		0.5	0.5
Anodic transfer coefficient of electrochemical reactions		0.5	0.5
Initial Li ion in sold phase	mol/m^3	1000	1000
Diffusion coefficient of liquid phase	m^2/s	7.5×10^{-14}	7.5×10^{-14}
Transference number of Li ion		0.363	0.363
specific heat capacity	$\text{J}.\text{kg}^{-1}\text{K}^{-1}$	700	700
thermal conductivity	$\text{W}.\text{m}^{-1}.\text{K}^{-1}$	2.10E+00	1.7
SEI resistivity	Ohm.m	5.00E+06	
Inner SEI lithium interstitial diffusivity	$\text{m}^2.\text{s}^{-1}$	1.00E-20	
Outer SEI solvent diffusivity	$\text{m}^2.\text{s}^{-1}$	2.50E-22	
SEI kinetic rate constant	$\text{m}.\text{s}^{-1}$	1.00E-12	
SEI open-circuit potential	V	0.4	
Li-plating rate constant	$\text{m}.\text{s}^{-1}$	1.00E-10	
Faraday constant (F)	$\text{C}.\text{mol}^{-1}$		
Gas constant	$\text{J}.\text{mol}^{-1}\text{K}^{-1}$		

Notes and references

- 1 M. Doyle, T. F. Fuller and J. Newman, *Journal of the Electrochemical society*, 1993, **140**, 1526.
- 2 T. F. Fuller, M. Doyle and J. Newman, *Journal of the electrochemical society*, 1994, **141**, 1.
- 3 J. Newman and N. P. Balsara, *Electrochemical systems*, John Wiley & Sons, 2021.
- 4 Z. Yan and M. Obrovac, *Journal of Power Sources*, 2018, **397**, 374–381.
- 5 C. J. Orendorff, G. Nagasubramanian, T. N. Lambert, K. R. Fenton, C. A. Apblett, C. R. Shaddix, M. Geier and E. P. Roth, *Sandia Report SAND*, 2012, **9186**, 2012.
- 6 E. Foreman, W. Zakri, M. Hossein Sanatimoghaddam, A. Modjtahedi, S. Pathak, A. G. Kashkooli, N. G. Garafolo and S. Farhad, *Advanced Sustainable Systems*, 2017, **1**, 1700061.
- 7 P. Arora, R. E. White and M. Doyle, *Journal of the Electrochemical Society*, 1998, **145**, 3647.
- 8 X.-G. Yang, Y. Leng, G. Zhang, S. Ge and C.-Y. Wang, *Journal of Power Sources*, 2017, **360**, 28–40.
- 9 C. M. Snyder, *The Rate Dependency of Li-ion Battery Degradation Mechanisms.*, Sandia national lab.(snl-nm), albuquerque, nm (united states) technical report, 2016.
- 10 Y. Jeon, H. K. Noh and H.-K. Song, *Scientific reports*, 2017, **7**, 1–9.
- 11 G. Sikha, B. N. Popov and R. E. White, *Journal of the Electrochemical Society*, 2004, **151**, A1104.
- 12 J. Vetter, P. Novák, M. R. Wagner, C. Veit, K.-C. Möller, J. Besenhard, M. Winter, M. Wohlfahrt-Mehrens, C. Vogler and A. Hamouche, *Journal of power sources*, 2005, **147**, 269–281.
- 13 T. R. Ferguson, *Ph.D. thesis*, Massachusetts Institute of Technology, 2014.
- 14 T.-T. Nguyen, A. Demortière, B. Fleutot, B. Delobel, C. Delacourt and S. J. Cooper, *npj Computational Materials*, 2020, **6**, 1–12.
- 15 J. Landesfeind, J. Hattendorff, A. Ehrl, W. A. Wall and H. A. Gasteiger, *Journal of The Electrochemical Society*, 2016, **163**, A1373.
- 16 B. Tjaden, D. J. Brett and P. R. Shearing, *International Materials Reviews*, 2018, **63**, 47–67.
- 17 P. Ramadass, B. Haran, P. M. Gomadam, R. White and B. N. Popov, *Journal of the Electrochemical Society*, 2004, **151**, A196.
- 18 V. R. Subramanian, V. D. Diwakar and D. Tapriyal, *Journal of The Electrochemical Society*, 2005, **152**, A2002.
- 19 R. Deshpande, M. Verbrugge, Y.-T. Cheng, J. Wang and P. Liu, *Journal of the Electrochemical Society*, 2012, **159**, A1730.
- 20 R. Timms, S. G. Marquis, V. Sulzer, C. P. Please and S. J. Chapman, *SIAM Journal on Applied Mathematics*, 2021, **81**, 765–788.
- 21 S. G. Marquis, R. Timms, V. Sulzer, C. P. Please and S. J. Chapman, *Journal of The Electrochemical Society*, 2020, **167**, 140513.